Applied Catalysis A: General 539 (2017) 29–37

Applied Catalysis A: General

journal homepage: www.elsevier.com/locate/apcata

Feature Article

Deactivation study of the hydrodeoxygenation of *p*-methylguaiacol over silica supported rhodium and platinum catalysts

F.P. Bouxin[a,b,*], X. Zhang[c], I.N. Kings[d], A.F. Lee[c], M.J.H. Simmons[d], K. Wilson[c], S.D. Jackson[a,**]

[a] Centre for Catalysis Research, School of Chemistry, University of Glasgow, Glasgow G12 8QQ, Scotland, UK
[b] Joint BioEnergy Institute, Lawrence Berkeley National Lab, Emeryville, 94608, USA
[c] European Bioenergy Engineering, University of Aston, Birmingham B4 7ET, UK
[d] School of Chemical Engineering, University of Birmingham, Birmingham B15 2TT, UK

ARTICLE INFO

Article history:
Received 22 December 2016
Received in revised form 23 March 2017
Accepted 29 March 2017
Available online 31 March 2017

Keywords:
Hydrodeoxygenation
p-Methylguaiacol
Rhodium
Platinum
Deactivation

ABSTRACT

Hydrodeoxygenation of *para*-methylguaiacol using silica supported Rh or Pt catalysts was investigated using a fixed-bed reactor at 300 °C, under 4 barg hydrogen and a WHSV of 2.5 h^{-1}. The activity, selectivity and deactivation of the catalysts were examined in relation to time on stream. Three catalysts were tested: 2.5% Rh/silica supplied by Johnson Matthey (JM), 2.5% Rh/silica and 1.55% Pt/silica both prepared in-house. The Rh/silica (JM) showed the best stability with steady-state reached after 6 h on stream and a constant activity over 3 days of reaction. In contrast the other two catalysts did not reach steady state within the timeframe of the tests, with continuous deactivation over the time on stream. Nevertheless higher coking was observed on the Rh/silica (JM) catalyst, while all three catalysts showed evidence of sintering. The Pt catalyst (A) showed higher selectivity for the production of 4-methylcatechol while the Rh catalysts were more selective toward the cresols. In all cases, complete hydrodeoxygenation of the methylguaiacol to methylcyclohexane was not observed.

1. Introduction

Bio-oils upgrading can be performed using a variety of different approaches. In order to blend with crude oil, or to drop-in to existing petroleum processes, the oxygen content (30–50%) of the bio-oil has to be reduced. Deoxygenation of the bio-oils can be achieved using a zeolite cracking approach [1] or catalytic hydrodeoxygenation [2,3]. Reductive media such as hydrogen or a hydrogen donor solvent are typically used for hydrodeoxygenation or the hydrogen transfer reaction. While hydrodeoxygenation of bio-oils has been studied for decades, the catalytic mechanisms and reasons for catalyst deactivation are still not fully understood [4]. The chemical composition of the bio-oils is extremely complex and depends on the amount of cellulose, hemicelluloses and lignin in the biomass feedstock and the pyrolysis conditions. During the pyrolytic process, celluloses and hemicelluloses produce sugars and furans which undergo additional decomposition to generate esters, acids, alcohols, ketones and aldehydes [2]. The phenolic compounds (phenols, guaiacols and syringols) are produced from the lignin component.

Amongst all the compounds present in the bio-oil, the phenolics are by far the most studied. The reasons are their multiple functional groups, their high proportion in the bio-oil and their tendency to promote catalyst deactivation. Another reason of the extensive use of phenolics as model compounds for bio-oil upgrading relies on the higher bond dissociation energy required to break aryl-hydroxyl or aryl-methoxy linkages compared to alkyl hydroxyl or alkyl ether linkages [5]. Within the pyrolysis of aromatic compounds, guaiacol has received the most attention [6,7]. During the upgrading process, guaiacol can undergo demethoxylation, demethylation and partial or complete hydrogenation.

Various catalysts have been studied for the hydrodeoxygenation of guaiacol. In a previous study, noble metals catalysts such as Pt, Pd or Rh, when compared to conventional sulfided $CoMo/Al_2O_3$, showed better performance and exhibited a lower carbon deposit [8]. A comparative study of Pt/Al_2O_3, Rh/Al_2O_3 and presulfided NiMo catalysts for the HDO of microalgae oil reported the better stability of the noble metal catalysts reaching a steady state after 5 h time on stream. The NiMo catalyst which did not reach steady state

* Corresponding author at: Joint BioEnergy Institute, Lawrence Berkeley National Lab, Emeryville, 94608, USA.
** Corresponding author.
E-mail addresses: flobou@lbl.gov, florentbouxin@hotmail.fr (F.P. Bouxin), david.jackson@glasgow.ac.uk (S.D. Jackson).

http://dx.doi.org/10.1016/j.apcata.2017.03.039
0926-860X/

after 7 h reaction was prone to higher carbon deposition [9,10]. Catalyst supports also play a significant role in the stability of the catalysts. Previous works reported that use of basic magnesia supports reduced the coking of the catalyst when compared to acidic alumina supports [11].

In this paper we report on the HDO reaction of *p*-methylguaiacol (PMG) over silica-supported rhodium and platinum catalysts. Silica was selected as the catalyst support for this study due to its less acidic properties with the aim of reducing carbon deposition.

Instead of guaiacol, HDO was performed using *p*-methylguaiacol as the model compound, as it is one of the main components of the pyrolytic oil formed from lignocellulosic feedstocks. Also unlike guaiacol, the methylation in the para position allowed discrimination of different reaction pathways via the generation of *m*- or *p*-cresol as illustrated in Fig. 1. The complete list of product names was given in Table S.1. Two 2.5% Rh/silica catalysts and a 1.55% Pt/silica catalyst were tested for this study.

2. Experimental

2.1. Materials

p-Methylguaiacol (PMG) and reference products were purchased from Sigma-Aldrich. A 2.5% Rh/SiO_2 catalyst was obtained from Johnson Matthey and prepared by incipient-wetness impregnation rhodium chloride salt on a Grace-Davison silica support (catalyst reference M02026). A 1.55% Pt/SiO_2 and a 2.5% Rh/SiO_2 catalysts were prepared by incipient-wetness impregnation of aqueous ammonium tetrachloroplatinate(II) (Alfa Aesar, 99.9%, $(NH_4)_2PtCl_4$) and Rhodium (III) chloride, (Sigma, 99.9%, $RhCl_3$, xH_2O) over fumed silica (Sigma-Aldrich, 0.2–0.3 mm avg. part. Size). Detailed protocols for Pt/SiO_2 (A) and Rh/SiO_2 (A) catalysts prepared by Aston University was described in previous work [12]. Each catalyst was ground and sieved to between 350 and 850 μm before use. The characteristics of the catalysts are listed in Table 1. All other reagents and solvents were purchased from Sigma-Aldrich and used without further purification.

2.2. Design of the fixed-bed unit

In a previous study, the eluent gas stream of guaiacol HDO was quantified using on-line GC analysis [13]. However in our system the complexity of the HDO products mixture (see Fig. 1) was not compatible with on-line GC analysis of the deoxygenated/hydrogenated oil. For example, para and *meta*-cresols could only be GC-differentiated after a silylation step.

Therefore a collector was required to sample the condensable products at different time on stream without interrupting the reaction. In a previous paper the liquid products were collected by bubbling the vaporised products into a cold liquid such as isopropanol [7]. This technique has the advantage to give an absolute value for each product, however this technique was felt more suitable for a low pressure system. In the present study, liquefaction of the product gas stream was obtained after passing through a condenser at 5 °C. As illustrated in Fig. 2, after passing through the condenser, the gas-liquid were separated and the liquid collected by gravitation into a ¼ inch stainless steel tubing before filling the collector from the bottom. A system of valves permitted isolation of the collector for sampling without disturbing the pressure of the system. The light products were also collected into a U-shape pipe, cooled to −60 °C connected after the pressure relief valve. The analysis of the light trap showed that only 5% of the toluene (lightest compound detected) was not condensed after passing through the condenser. No other products were detected to have passed the condenser in the gas phase except a trace of *p*-methylguaiacol (PMG) due to its large excess in the product stream.

However, due to the lack of precision on the sampling volume (liquid hold-up in the condenser), an exact mass balance and an absolute quantification of each product could not achieved. As consequence, only a relative molar quantification of products was performed with the conversion, yield and selectivity as defined in Eqs. (1)–(3):

$$\text{Conversion} = (\Sigma\text{moles of products})/(\Sigma\text{products} + \text{molof PMG out}) \quad (1)$$

$$\text{Yield} = \text{mol of product (i)}/(\Sigma\text{moles of products} + \text{molofPMGout}) \quad (2)$$

$$\text{Selectivity} = \text{mol of product (i)}/\Sigma\text{moles of products} \quad (3)$$

2.3. Catalytic hydrodeoxygenation of p-methylguaiacol

The catalytic test was performed in a continuous-flow, fixed-bed reactor over 0.45 g of silica supported noble metal catalyst. Similar catalyst bed volumes of 0.84–0.88 cm^{-3} were estimated from the bulk densities of the catalysts of 0.51, 0.52 and 0.54 g cm^{-3} for the Rh/SiO_2 (A), Pt/SiO_2 (A) and Rh/SiO_2 (JM), respectively. With a reactor inner diameter of 0.40 cm, the bed catalyst length was around 6.7–7.0 cm. The catalyst was pre-reduced in-situ before reaction at 300 °C for 2 h under 100 mL min^{-1} of 40% H_2/Argon. After the catalyst was reduced, *p*-methylguaiacol (PMG) was pumped into the gas flow and vaporised at 200 °C. The reaction temperature was 300 °C with a hydrogen partial pressure of 4 barg giving a H_2:PMG molar ratio of 15. The total pressure was made up to 10 barg using argon. The weight hourly space velocity (WHSV) of PMG was 2.5 h^{-1}, while the gas hourly space velocity (GHSV) was 7200 h^{-1} with gas flow rate of 100 mL min^{-1}. Gas mass flow controllers were used to feed hydrogen and argon while a Gilson HPLC pump was used to feed the *p*-methylguaiacol. In order to avoid condensation, gas lines before and after the reactor were heated to 220 °C. A condenser at 5 °C was used to liquefy the products before sampling. The HDO products (100–200 mg) were diluted in 5 mL of dichloromethane (DCM).

2.4. Analysis of the oily products

2.4.1. Analytes preparation

In order to fully quantify the products and due to the significant variation of products' abundance, three distinct solutions were prepared from the same mixture of products/internal standards (IS). First, an aliquot of the HDO products in DCM (100 μL) was mixed with 50 μL of IS (C10 at 0.86 and C17 at 10.2 g L^{-1}). Then, 20 μL of this mix was silylated while the remaining mixture was diluted with 0.5 mL of dichloromethane. Finally, 5–10 μL of the diluted solution was also silylated to quantify the PMG, methylcatechol and cresol products. The non-silylated solutions were injected to quantify the light products such as methylcyclohexane and toluene but also the 4-methyl-2-methoxycyclohexanone which co-eluted with the trimethylsilyl methylcyclohexanol. This technique permitted a full quantification of minor and major products.

2.4.2. GC/FID experimental conditions

Qualitative analyses of the HDO products were performed on a Shimadzu GC-2010 coupled to a MS-QP2010S. Samples were injected on a ZB-5MS capillary column (30 m × 0.25 mm × 0.25 μm). The quantitative analyses were performed on an HP 5890 gas chromatograph fitted with a Supelco DB-5 capillary column (30m × 0.32 mm, 1 mm thickness). Quantification was obtained using decane C10 and heptadecane C17 as internal standards and the relative response coefficients were based on exact products when possible or on response coefficients of similar product structure for non-commercial products.

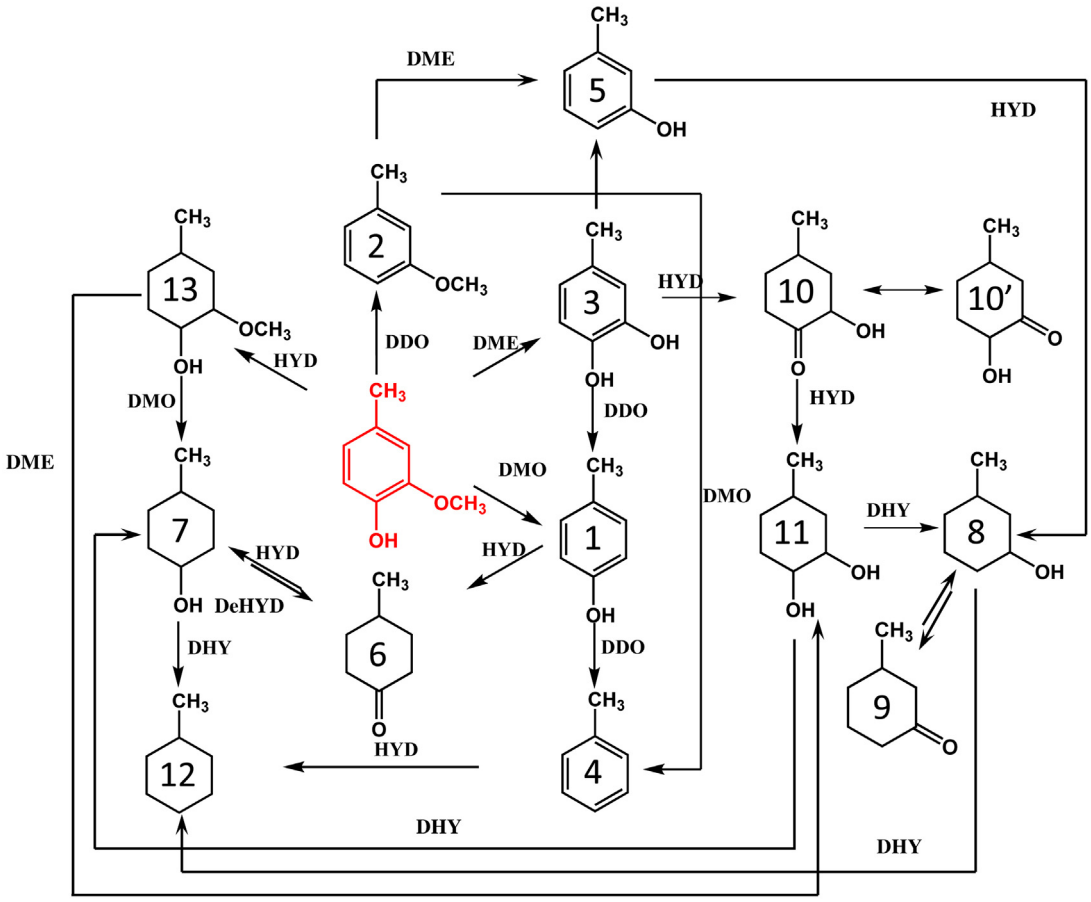

Fig. 1. Reaction pathways for the HDO of *p*-methylguaiacol. [DMO: demethoxylation, DME: demethylation, DDO: direct deoxygenation, HYD: hydrogenation, DeHYD: dehydrogenation, DHY: dehydration].

Table 1
Catalyst characterisation before and after reaction.

	Catalyst surface area/$m^2\ g^{-1}$	Metal crystallite size/nm	Metal surface area/$m^2\ g^{-1}$	Metal dispersion/%	Carbon content/%
1.55%Pt-SiO_2 (A)	242	15	0.83	7.2	0.1
1.55%Pt-SiO_2 (A) Post Reaction	167	23	0.31	4.8	5.7
2.5%Rh-SiO_2 (A)	234	16	4.15	6.8	0.1
2.5%Rh-SiO_2 (A) Post Reaction	189	18	3.90	6.1	4.9
2.5%Rh-SiO_2 (JM)	473	40	2.04	2.8	0.2
2.5%Rh-SiO_2 (JM) Post Reaction	269	43	1.31	2.6	13.1

2.5. Catalysts characterization

2.5.1. Temperature programmed oxidation analysis

Temperature programmed oxidation (TPO) was carried out using a combined TGA/DSC SDT Q600 thermal analyser coupled to an ESS mass spectrometer for evolved gas analysis. A sample loading of 10–15 mg was used and samples were typically heated from 30 °C to 900 °C using a ramp rate of 10 °C min^{-1} under 2% O_2/Ar, with a flow rate of 100 mL min^{-1}. For mass spectrometric analysis, various mass fragments were followed such 18 (H_2O), 28 (CO), and 44 (CO_2). All TGA work was kindly carried out by Andy Monaghan at the University of Glasgow.

2.5.2. Surface area and pore volumes distribution

Nitrogen porosimetry was conducted on the Quantachrome Nova 4000e porosimeter and analysed with the software of NovaWin version 11. Samples were degassed at 120 °C for 2 h under vacuum conditions prior to analysis by nitrogen adsorption at −196 °C. Adsorption/desorption isotherms were recorded for all parent and Pt-impregnated and Rh-impregnated silicas. The BET (Brunauer-Emmett-Teller) surface areas were derived over the relative pressure range between 0.01 and 0.2. Pore diameters and volumes were calculated using the BJH method according to desorption isotherms for relative pressures >0.35.

2.5.3. Metal dispersion and surface areas

Pt and Rh dispersions were measured via CO pulse chemisorption on a Quantachrome ChemBET 3000 system. Samples were outgassed at 150 °C under flowing He (20 mL min^{-1}) for 1 h, prior to reduction at 150 °C under flowing hydrogen (10 mL min^{-1}) for 1 h before room temperature analysis (this reduction protocol is milder than that employed during Pt or Rh impregnation and does not induce particle sintering). A CO:Pt surface stoichiometry of 0.68 was assumed according to the literature [14,15]; the CO-Rh interaction was much more complicated because the CO bond is very sensitive to the particular electron distribution, such as the spin-states and the initial occupations of the Rh 5 s electronic states [16]; therefore, the CO:Rh ratio was difficult to determine. For estima-

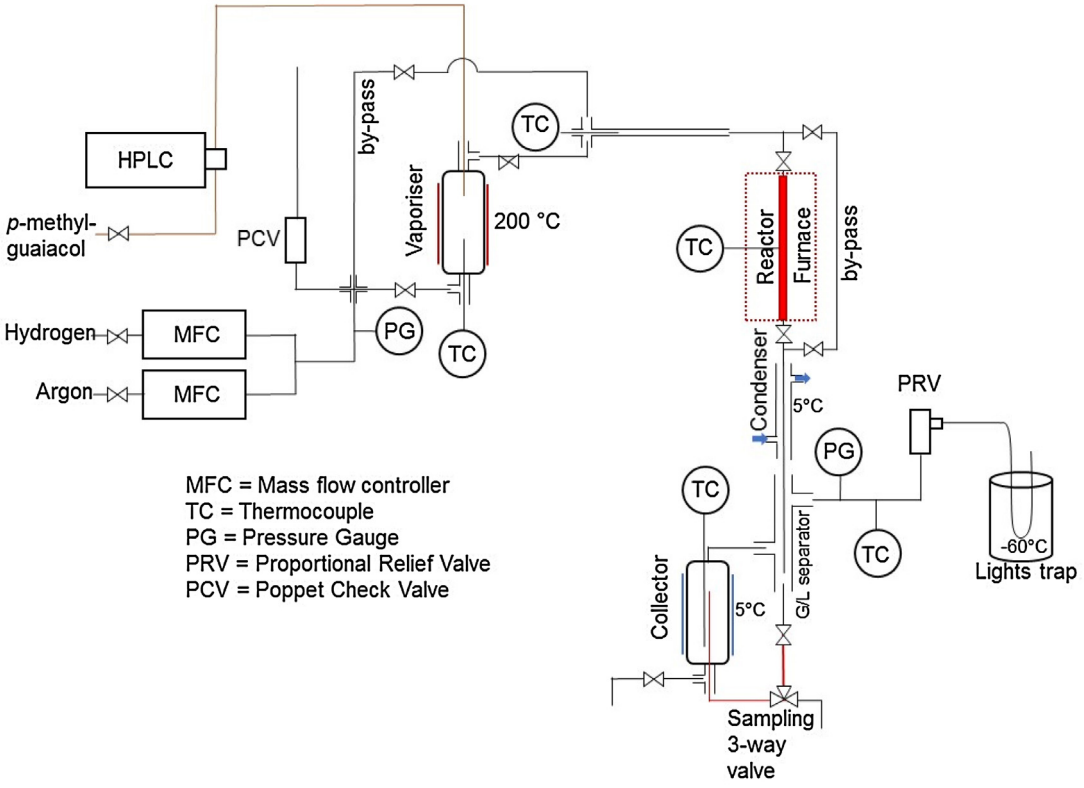

Fig. 2. Fixed bed reactor experimental set-up.

tion, a CO:Rh surface stoichiometry of 1 could be assumed on the basis of literature [16,17].

2.5.4. CHNS elemental analysis

Carbon loadings (accumulated on the spent catalysts) were obtained using a Thermo Flash 2000 organic elemental analyser, calibrated to a sulphanilimide standard, with the resulting chromatograms analysed using Thermo Scientific's Eager Xperience software. Vanadium pentoxide was added to aid sample combustion.

2.5.5. Raman spectroscopy analysis

Raman spectra of post reaction catalysts were obtained with a Horiba Jobin Yvon LabRAM High Resolution spectrometer. A 532.17 nm line of a coherent Kimmon IK series He-Cd laser was used as the excitation source for the laser. Laser light was focused for 10 s using a 50× objective lens and grating of 600. The scattered light was collected in a backscattering configuration and was detected using nitrogen cooled charge-coupled detector. A scanning range of 100 and 4100 cm^{-1} was used.

3. Results/discussion

3.1. p-*Methylguaiacol conversion and selectivity*

The activity/selectivity of the three catalysts was studied with the time on stream. The main purpose of these experiments was to determine if the catalyst activity reached a steady state or if deactivation was continuous. Low activity of the catalyst was not an issue but identification of the variation of catalyst activity and product selectivity were critical for a future kinetic study of the hydrodeoxygenation of *p*-methylguaiacol. Catalyst testing was performed at 300 °C, a WHSV of 2.5 h^{-1}, 4 barg hydrogen and a H_2:PMG molar ratio of 15:1. The rhodium/silica (JM) catalyst and both Rh/silica (A) and Pt/SiO_2 (A) catalysts were studied over several days (see Fig. 3). Rh/SiO_2 (JM) showed fast deactivation initially but this was followed by a period of constant activity, whereas although the Rh/SiO_2 (A) showed the same deactivation profile initially, no steady state was observed. The deactivation profile of the Pt/SiO_2 catalyst was different from that of the rhodium catalysts in that it exhibited a constant loss of activity. This linear deactivation has previously been reported on HDO of guaiacol over Pt/Al_2O_3 and Pt/MgO [11].

The deactivation of the Pt/silica was plotted (Fig. 4) using the relationship, $\ln[X_{t0}/(1-X_t)] = \ln(k\tau_w) - k_d t$, where, X_t is the conversion the reactant at time t, k is the rate constant, τ_w represents weight time, k_d the deactivation rate constant and t is time [18].

The deactivation plot gave a deactivation rate constant of 0.02 h^{-1} (R^2 = 0.92). However, the Rh/Silica (A) data fitted a logarithmic curve with regression coefficient (R^2) of 0.99 which showed that the deactivation mechanism was not time independent.

The catalysts initial selectivity and those after ~12 h and ~32 h TOS are shown in Fig. 5. Compared to the Pt/SiO_2 (A) and the Rh/SiO_2 (A), the Rh/SiO2 (JM) was the only catalyst that showed constant selectivity from 10 h to 33 h TOS. After 32 h on stream, 42 mol% of the products were *p*-methylcatechol with Rh/SiO_2 (A) whereas with Rh/SiO_2 (JM) the selectivity to *p*-methylcatechol was only 12 mol%. This significant variation may be explained by the different nature of silica support used. As illustrated in Fig. 6, Rh/SiO_2 (A) produced *p*-methylcatechol with the same rate from 12 to 72 h TOS. While deoxygenation and hydrogenation reaction were deactivated over time, the demethylation of the PMG was not affected. The high demethylation activity for the Rh/silica (A) can be suggested by higher acidity of the silica support. For the Pt/SiO_2 (A), the selectivity toward the 4-methyl catechol increased from 8 to 25 mol% from 1 h to 32 h TOS while the selectivity toward the *m*- and *p*-cresol decreased from 22.6 and 40.1 mol% to 13.6 and 34.0 mol%.

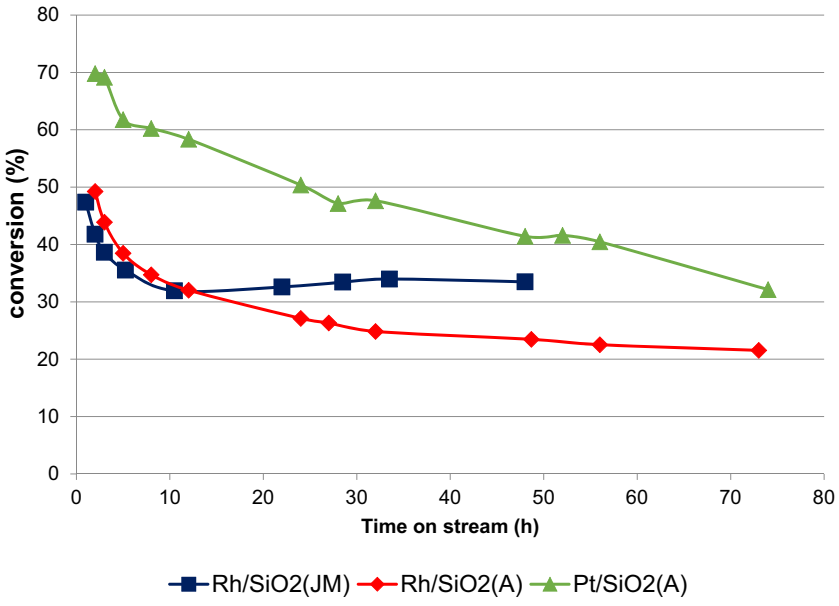

Fig. 3. *p*-Methylguaiacol conversion at 300 °C, 4 barg hydrogen, WHSV of 2.5 h^{-1} and H_2/PMG molar ratio of 15.

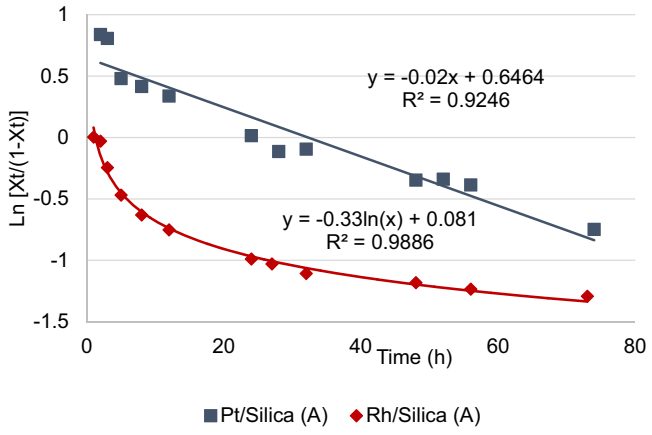

Fig. 4. Deactivation plot for Pt/silica and Rh/silica (A).

Comparing the two rhodium catalysts some notable differences are observed. Initially the Rh/silica (A) shows a high selectivity to toluene and a low selectivity to 4-methyl catechol but by 32 h TOS the selectivity has reversed. This behaviour raises the question as to whether it is possible to remove two —OH groups before desorption, effectively by-passing the formation of *p*-cresol as an intermediate. This behaviour is not seen with the Rh/silica (JM) catalyst where the selectivity is relatively unchanged over the TOS. There are two significant differences between the rhodium catalysts. Different silica supports were used and the metal crystallite size is different (Table 1). Their preparations were identical so the significant difference of products selectivity between the two rhodium catalysts could be attributed to either the nature of the silica support or a metal particle size effect. A more in-depth investigation of these effects will be required to fully interpret these changes in selectivity.

3.2. *Yields of* p-*cresol,* m-*cresol and 4-methylcatechol as function of time*

The variations of the molar yield of the principle products (those with yields >2 mol%) are shown in Fig. 6 for the three catalysts. With Rh/SiO_2 (JM) and Pt/SiO_2 (A) catalysts *p*-cresol was the main product. For the Rh/SiO_2 (A), *p*-cresol was the main product for the first 24 h TOS, subsequently methylcatechol was the main product. As illustrated in Fig. 6, Pt/Silica (A) showed similar conversion rate of *p*-methylguaiacol to 4-methyl catechol than Rh/Silica (A) from 24 h to 72 h. However, the Pt/silica catalyst showed a different deactivation profile for the three main products (*p*-cresol, *m*-cresol and 4-methylcatechol), with the yield of 4-methylcatechol decreasing more slowly than the yields of both *para*- and *meta*-cresol suggesting that catalyst deactivation affected the demethylation of the *p*-methylguaiacol less than the demethoxylation and direct deoxygenation. Platinum has been reported to favour the demethylation of guaiacol and this could explain the high demethylation activity in the early stages [19]. In the case of both Rh catalysts, there was low conversion of *p*-methylguaiacol to 4-methylcatechol initially, which then increased and stabilized to a constant production after 10 h or 5 h on stream for Rh/silica (A) or Rh/silica (JM) respectively. Indeed, for the Rh/silica (A) catalyst, 4-methylcatechol becomes the principal product. This is explained by the concomitant loss of deoxygenation of the methylcatechol to *m*- or *p*-cresol. The yields of the *p*-cresol and *m*-cresol also stabilized after 10 h on stream for the Rh/silica (JM) catalyst consistent with it achieving steady state. On the other hand, the Rh/silica (A) and Pt/silica did not reach a steady state within the time of the study. It could be speculated that Rh/silica (A) required a longer reaction time in order to reach a steady state as illustrated by the deactivation profile in Fig. 3. However, in the case of the Pt/silica catalyst, the continuous deactivation profile suggested that the catalyst may not reach a steady state condition. Extended testing would be required to determine whether a low activity steady state was reached or whether the system was subject to continuous deactivation. As illustrated in Fig. 1, the production of *m*-cresol or *p*-cresol required the demethylation and direct deoxygenation. The *p*-cresol can also be produced directly from the demethoxylation of the methylguaiacol. As illustrated in Figure S.1, the ratios *p*-cresol/*m*-cresol were 3.1, 2.4 and 2.2 after 12 h TOS for Rh (JM), Rh (A) and Pt (A) catalysts, respectively. The production of *p*-cresol via demethoxylation was more pronounced in the case of the Rh (JM) and can be explained by the low activity of the catalyst toward demethylation. On the other hand, the Rh (A) and Pt (A) catalysts produced a *p*-cresol/*m*-cresol ratio closer to two suggesting that both demethoxylation and demethylation/direct deoxygenation pathways were more bal-

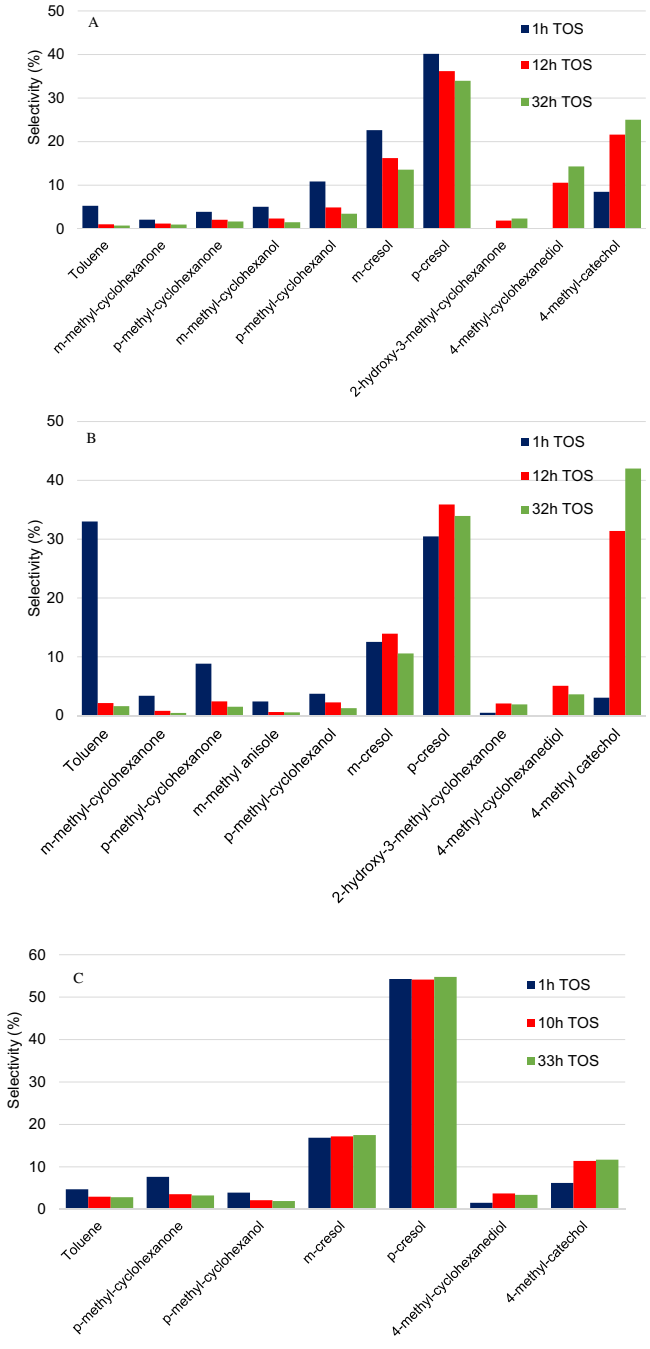

Fig. 5. Selectivity obtained from (A) Pt/silica, (B) Rh/silica (A) at 1 h, 12 h and 32 h TOS and (C) Rh/silica (JM) at 1 h, 10 h and 33 h TOS (only compounds with selectivity >2% are reported).

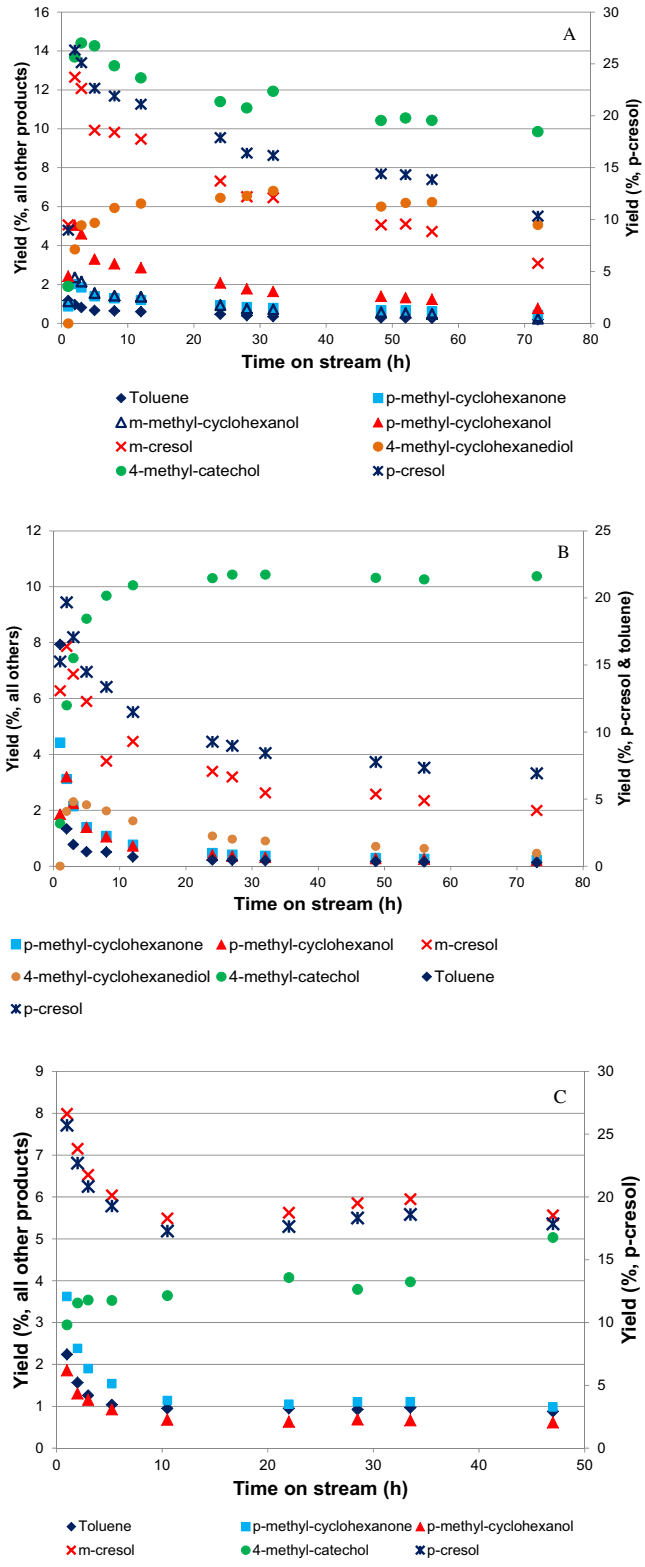

Fig. 6. Variation of product yield with time over (A) Pt/silica, (B) Rh/silica (A) and (C) Rh/silica (JM). Conditions: 300 °C, 4 bar hydrogen, WHSV of 2.5 h^{-1} and H_2/PMG molar ratio of 15.

anced. This can be explained by the higher activity of both catalysts toward the demethylation (Fig. 6). However, while the Rh (JM) showed a constant ratio between the *m*- and *p*-cresol, the Rh (A) and Pt (A) showed an increase of the ratio with TOS. As consequence, the pathways for the production of *m*-cresol and *p*-cresol were not affected the same way with the deactivation of the Pt (A) and Rh (A) catalysts. It could be suggested that the demethoxylation was less affected than the direct deoxygenation. However, different rate of hydrogenation of the *p*-cresol and *m*-cresol could also explained this difference and will be discussed in the next section.

3.3. *Hydrogenation of* p*-cresol,* m*-cresol and methylcatechol as function of the time*

Hydrogenation can be affected differently according to the nature of the intermediate products and the catalyst used. Accord-

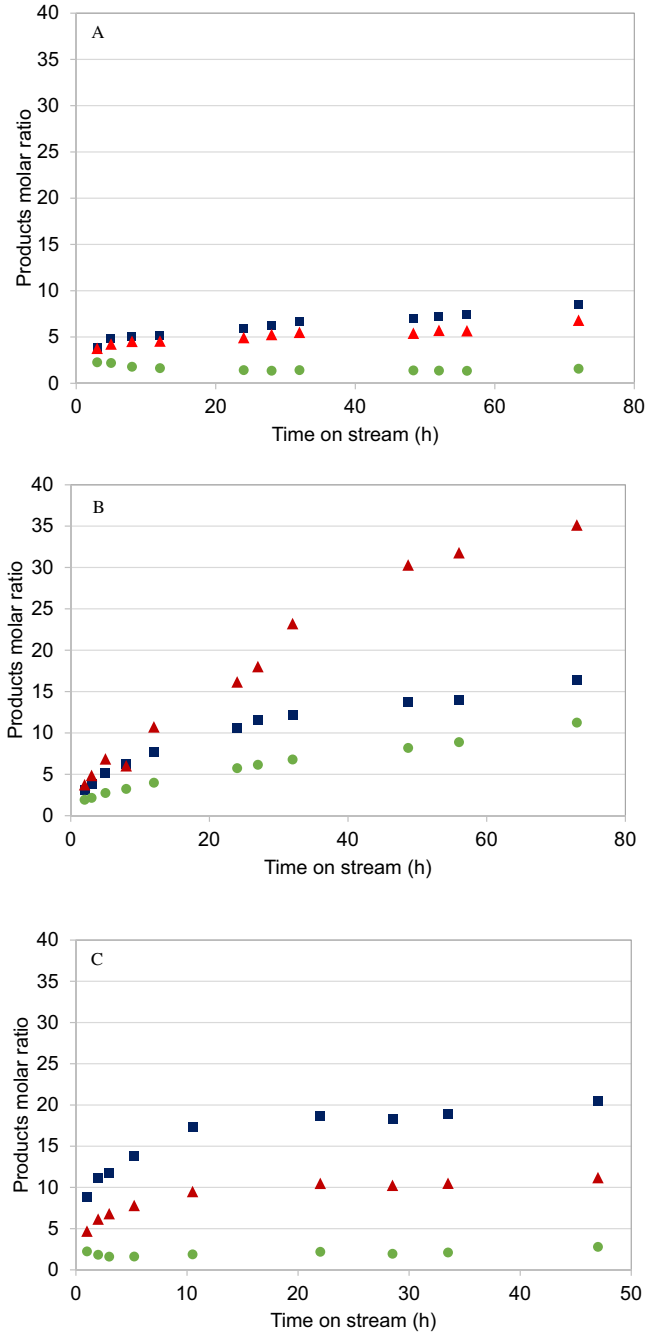

Fig. 7. Molar ratio of (blue square) *p*-cresol (1)/hydrogenated *p*-cresol products(6–7), (red triangle) m-cresol (5)/hydrogenated m-cresol products (8–9) and (green dot) methylcatechol (3)/hydrogenated methylcatechols products (10–11) as function of the time on stream at 300 °C, 2.5 WHSV, 4 bar of H_2 and H_2/PMG molar ratio of 15 [A:1.55%Pt/SiO_2 (A); B: 2.5%Rh/SiO_2 (A); C: 2.5%Rh/SiO_2 (JM)]. (For interpretation of the references to colour in this figure legend, the reader is referred to the web version of this article.)

ing to the reaction pathways illustrated in Fig. 1, the molar ratio of *p*-cresol (1), *m*-cresol (5), *p*-methylcatechol (3) and the hydrogenated products of the *p*-cresol (6–7), *m*-cresol (8–9), *p*-methylcatechol (10–11) was calculated for the three catalysts. As illustrated in Fig. 7A, the hydrogenation of the *p*-cresol and *m*-cresol on the Pt/silica (A) catalyst was in the same range and followed the same loss of activity. From 3 h to 72 h on stream the ratio increased from 3.9 and 3.7 to 8.5 and 6.4 for the *p*-cresol and *m*-cresol, respectively. In the case of both Rh catalysts (Fig. 7B and C), the hydrogenation rate of *m*-cresol was around twice the rate of hydrogenation of the *p*-cresol after 48 h. For the Rh/silica (A) catalyst, while the loss of hydrogenation activity for the *p*-cresol was in the same range than for Pt/silica catalyst, the loss of hydrogenation activity related to *m*-cresol was far more pronounced. Finally, the Rh/silica (JM) catalyst showed a loss of hydrogenation activity for both cresols up to 10 h on stream followed with a constant ratio around 18 and 10 for *p*-cresol and *m*-cresol.

As illustrated in Fig. 7, the evolution of 4-methylcatechol hydrogenation was less affected for the Pt/silica (A) and Rh/silica (JM) catalysts than the Rh/silica (A) catalyst. In the case of Rh/silica (A), the molar ratio of methylcatechol(5):hydrogenated products of methylcatechol (10–11) increased from 2 to 9 after 56 h on steam while the ratio only increased from 2 to 2.8 for Rh/silica (JM). In contrast, the ratio slightly decreased from 2.2 to 1.4 for the Pt catalyst. While the hydrogenation of the cresols over the Pt catalyst decreased with time on stream, the hydrogenation of the catechol inversely increased leading to a constant overall selectivity to hydrogenated products. In all cases, the ratio between non hydrogenated:hydrogenated products showed that the catalysts were more active for the hydrogenation of the methylcatechol than the cresols. This suggested that the presence of vicinal alcohol favoured the adsorption of the catechol on the catalysts.

3.4. Characteristics of the Pt and Rh post-reaction catalysts

Previous work had suggested that catalyst deactivation was due to carbon deposition on the surface of the catalyst with the initiation of coke formation suggested to be located at the acid site of the support [20]. As illustrated in Fig. 8, TPO analysis of the spent catalysts clearly showed the presence of carbonaceous deposits. It is interesting to note that the Rh/silica (JM) catalyst showed the highest amount of carbon laydown yet it reached a steady state in contrast to the other catalysts. It is also notable that the two catalysts with the same support show quite similar mass loss, which could be expected if the carbon deposit was principally associated with the support. The extent of overall carbon laydown however is very low when considered as a percentage of the feed. Over the Rh/silica (JM) 0.18% of the feed was deposited on the catalyst, while for Rh/silica (A) only 0.03% was deposited. Over Pt/silica (A) the amount deposited was only 0.04% of the feed.

Looking in detail at the TPO the Rh/silica (JM) catalyst showed mass loss at low temperature (~160 °C) suggesting the released of adsorbed species as there is no concomitant generation of carbon dioxide. There are weight losses resulting in carbon dioxide evolution at ~250 °C and 300 °C. At these temperatures the surface species are likely to be pseudo-molecular with a significant H:C ratio. There are then two weight loss events at 445 °C and 469 °C, which are accompanied with carbon dioxide evolution. These weight losses reveal the presence of two similar carbonaceous deposits; the lower temperature species is unique to the Rh/silica (JM) catalyst, while the higher temperature event is common to all three catalysts. The rapidity of the weight loss at 469 °C indicates fast combustion of the deposit suggesting that this deposit is hydrocarbonaceous in nature and is associated with the metal. There is a further weight loss event at 583–640 °C, on all the catalysts, which is accompanied with carbon dioxide evolution. This high temperature weight loss can be associated with the combustion of graphitic species (Raman spectroscopy revealed a weak G-band at ~1590 cm^{-1} on all the catalysts) on the silica supports, which would be consistent with the loss in surface area as measured by BET (Table 1). The carbon content of the used catalysts was also determined by CHN analysis (Table 1) and showed the same trend as that found with the TGA. The surface area of the Rh/silica (JM) catalyst was nearly twice that of the Pt/silica and Rh/silica (A) catalysts which could explain the higher carbon deposition. Reduction

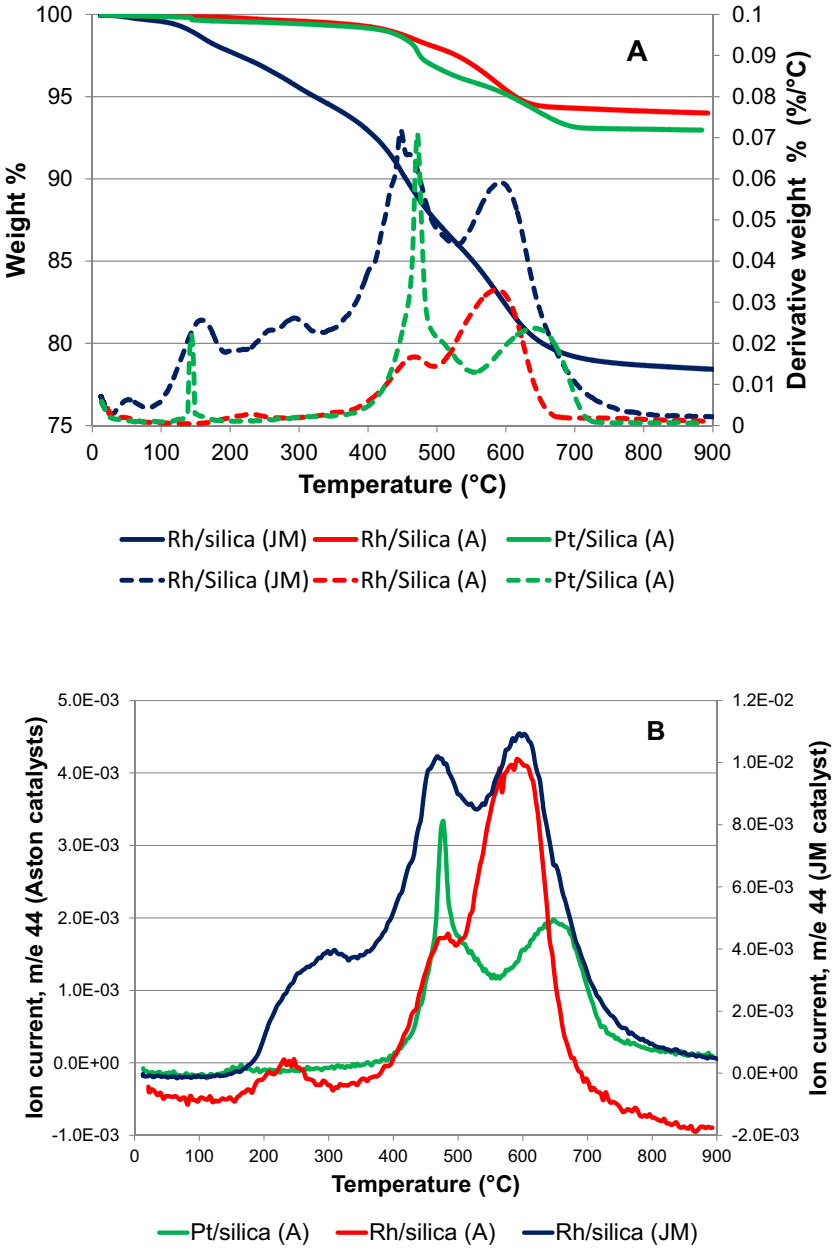

Fig. 8. TPO analysis (A) of the spent catalysts [blue: Rh/SiO_2(JM); red: Rh/SiO_2(A); green: Pt/SiO_2(A)] and CO_2-TPO profile (B).

of the surface areas of 20%, 30% and 43% for Rh (A), Pt (A) and Rh (JM) respectively, are attributed to the carbon blocking pores.

As illustrated in Table 1, after reaction the metal dispersion was reduced in all three catalysts. The Pt catalyst showed the largest drop with metal dispersion reducing from 7.2 to 4.8% and a concomitant increase in metal crystallite size. Sintering of Pt/silica catalysts under HDO conditions has been observed in a previous study and can be explained by a weak interaction between Pt and the silica support [21]. This sintering, in conjunction with the carbon laydown, would explain the continuing loss of activity of the Pt/silica catalyst. In contrast, the metal dispersion of the Rh/silica (JM) and Rh/Silica (A) was only reduced from 2.8 to 2.6 and from 6.8 to 6.1, respectively, indicating a much stronger interaction between support and Rh metal. Finally, by the end of the reaction, the metal surface area of the Rh/silica (A) was three times higher than that of the Rh/silica (JM) catalyst, yet the *p*-methylguaiacol conversion was lower, indicating that there was not a simple correlation between metal surface area and activity.

4. Conclusion

Both Rh/silica catalysts showed both similar deactivation profiles with a fast deactivation at early time on stream followed with slow deactivation for the Rh/silica (A) or constant activity for the Rh/silica (JM). The Pt/silica (A) catalyst showed continuous deactivation correlated with metal sintering and carbon laydown. The carbon deposit, higher in the case of the Rh/silica (JM) compared to the Pt and Rh/silica (A), could be explained by the different nature of the silica support. Detailed analysis of the product distributions with time revealed that the specific activity of the catalysts for demethylation, demethoxylation and hydrogenation were affected differently by the catalyst deactivation. The demethylation activity was the least affected by the catalyst deactivation, whereas hydrogenation activity was severely decreased for the Rh/silica (A) catalyst. This behaviour suggests that different sites are responsible for demethylation and hydrogenation activity. The Pt catalyst showed a shift of hydrogenation selectivity from cresols

to 4-methylcatechol and the production of 4-methyl cyclohexan-1,2-diol. TPO analysis of the deposited carbon revealed at least three carbonaceous species on the surface of the rhodium catalysts, while only two different carbon species were detected on the platinum catalyst. Only the Rh/silica (JM) reached a prolonged steady state after 10 h on stream and modelling of the kinetics of PMG HDO will be reported in a subsequent paper.

Acknowledgments

UK Catalysis Hub is kindly thanked for resources and support provided via our membership of the UK Catalysis Hub Consortium and funded by EPSRC (grants EP/K014706/1, EP/K014668/1, EP/K014854/1, EP/K014714/1 and EP/M013219/1). The authors thank Andy Monaghan for expert technical assistance.

Appendix A. Supplementary data

Supplementary data associated with this article can be found, in the online version, at http://dx.doi.org/10.1016/j.apcata.2017.03.039.

References

[1] O.D. Mante, F.A. Agblevor, Green Chem. 16 (2014) 3364–3377.
[2] M. Saidi, F. Samimi, D. Karimipourfard, T. Nimmanwudipong, B.C. Gates, M.R. Rahimpour, Energy Environ. Sci. 7 (2014) 103–129.
[3] Q. Bu, H. Lei, A.H. Zacher, L. Wang, S. Ren, J. Liang, Y. Wei, Y. Liu, J. Tang, Q. Zhang, R. Ruan, Bioresour. Technol. 124 (2012) 470–477.
[4] A.J. Ragauskas, G.T. Beckham, M.J. Biddy, R. Chandra, F. Chen, M.F. Davis, B.H. Davison, R.A. Dixon, P. Gilna, M. Keller, P. Langan, A.K. Naskar, J.N. Saddler, T.J. Tschaplinski, G.A. Tuskan, C.E. Wyman, Science (Washington, DC, USA) 344 (2014) 709.
[5] D.A. Ruddy, J.A. Schaidle, J.R. Ferrell III, J. Wang, L. Moens, J.E. Hensley, Green Chem. 16 (2014) 454–490.
[6] W. Mu, H. Ben, X. Du, X. Zhang, F. Hu, W. Liu, A.J. Ragauskas, Y. Deng, Bioresour. Technol. 173 (2014) 6–10.
[7] R.N. Olcese, M. Bettahar, D. Petitjean, B. Malaman, F. Giovanella, A. Dufour, Appl. Catal. B: Environ. 115–116 (2012) 63–73.
[8] A. Gutierrez, R.K. Kaila, M.L. Honkela, R. Slioor, A.O.I. Krause, Catal. Today 147 (2009) 239–246.
[9] L. Zhou, A. Lawal, Energy Fuels 29 (2015) 262–272.
[10] L. Zhou, A. Lawal, Catal. Sci. Technol. 6 (2016) 1442–1454.
[11] T. Nimmanwudipong, C. Aydin, J. Lu, R.C. Runnebaum, K.C. Brodwater, N.D. Browning, D.E. Block, B.C. Gates, Catal. Lett. 142 (2012) 1190–1196.
[12] X. Zhang, L.J. Durndell, M.A. Isaacs, C.M.A. Parlett, A.F. Lee, K. Wilson, ACS Catal. 6 (2016) 7409–7417.
[13] H.Y. Zhao, D. Li, P. Bui, S.T. Oyama, Appl. Catal. A: Gen. 391 (2016) 305–310.
[14] R. Chen, Z. Chen, B. Ma, X. Hao, N. Kapur, J. Hyun, K. Cho, B. Shan, Comput. Theor. Chem. 987 (2012) 77–83.
[15] S.R. Longwitz, J. Schnadt, E.K. Vestergaard, R.T. Vang, E. Lgsgaard, I. Stensgaard, H. Brune, F. Besenbacher, J. Phys. Chem. B 108 (2004) 14497–14502.
[16] T. Mineva, N. Russo, H.-J. Freund, J. Phys. Chem. A 105 (2001) 10723–10730.
[17] J. Liu, R. Tao, Z. Guo, J.R. Regalbuto, C.L. Marshall, R.F. Klie, J.T. Miller, R.J. Meyer, ChemCatChem 5 (2013) 3665–3672.
[18] R.J. Farrauto, C.H. Bartholomew, Fundamentals of Industrial Catalytic Processes, in: C.A. Hall (Ed.), 1997, pp. 306–311.
[19] R.C. Runnebaum, T. Nimmanwudipong, D.E. Block, B.C. Gates, Catal. Sci. Technol. 2 (2012) 113–118.
[20] M.D. Argyle, C.H. Bartholomew, Catalysts 5 (2015) 145–269.
[21] A.J. Foster, P.T.M. Do, R.F. Lobo, Top. Catal. 55 (2012) 118–128.